N92-24335

ACOUSTIC INTENSITY CALCULATIONS FOR AXISYMMETRICALLY MODELED FLUID REGIONS

by

Stephen A. Hambric and Gordon C. Everstine
Computational Mechanics Division (128)
David Taylor Research Center
Bethesda, MD 20084-5000

ABSTRACT

An algorithm for calculating acoustic intensities from a time-harmonic pressure field in an axisymmetric fluid region is presented. Acoustic pressures are computed in a mesh of NASTRAN triangular finite elements of revolution (TRIAAX) using an analogy between the scalar wave equation and elasticity equations. Acoustic intensities are then calculated from pressures and pressure derivatives taken over the mesh of TRIAAX elements. Intensities are displayed as vectors indicating the directions and magnitudes of energy flow at all mesh points in the acoustic field. A prolate spheroidal shell is modeled with axisymmetric shell elements (CONEAX) and submerged in a fluid region of TRIAAX elements. The model is analyzed to illustrate the acoustic intensity method and the usefulness of energy flow paths in the understanding of the response of fluid-structure interaction problems. The structural-acoustic analogy used is summarized for completeness. This study uncovered a NASTRAN limitation involving numerical precision issues in the CONEAX stiffness calculation causing large errors in the system matrices for nearly cylindrical cones.

INTRODUCTION

An acoustic intensity formulation for general, axisymmetric, fluid domains modeled with TRIAAX elements is presented. Numerical acoustic field solutions to fluid-structure interaction problems currently yield acoustic pressure fields, which may be used to locate high acoustic pressure concentrations. The motivation for calculating and displaying acoustic intensities is to help visualize the energy flow paths which cause high pressure regions. The energy flow fields can then help to identify dominant power paths which flow between structure and fluid, and therefore the important radiating parts of a structure.

The general problem of computing the interaction of an elastic structure with an acoustic fluid can be solved by combining a finite element model of the structure with a fluid loading computed using boundary element [1-11], finite element [12-23], combined finite element/analytical [24-26], T-matrix [27-29], and approximate fluid loading [30-32] techniques. In the fluid finite element approach, the exterior fluid domain is modeled with finite elements truncated at a finite distance from the structure and terminated with an approximate radiation boundary condition to absorb outgoing waves. The principal computational trade-off between this approach and the boundary element approach is that the finite element approach yields large, banded matrices, whereas the boundary element approach yields smaller, densely-populated matrices. This trade-off sometimes favors the finite element approach for long, slender structures like ships which are "naturally banded." In addition, only the fluid finite element approach has directly available an explicit fluid mesh which can be used for graphical display of the wave motion through the fluid. Since a significant part of our interest involves the display of wave propagation through both structure and fluid, we therefore formulate this problem using the fluid finite element approach. The principal drawbacks to fluid finite element modeling are the need for an approximate radiation boundary condition at the outer fluid boundary, the requirements on mesh size and extent (sometimes leading to frequency-dependent fluid meshes [20]), and the difficulty of generating the fluid mesh.

Direct frequency response NASTRAN [33] solutions for axisymmetric regions are described in general, and for domains that are defined using both structural and fluid subregions. Structural regions are modeled using standard structural finite elements (CONEAX, TRIAAX, TRAPAX); fluid regions are modeled with triangular elements of revolution (TRIAAX) using an analogy relating the Helmholtz equation to the elasticity equations used for the structural elements. The analogy is described in detail by Everstine [34] and is summarized for completeness here. The modeling of fluid-structure interaction between fluid and structure domains is also defined, as well as the application of acoustic boundary conditions to fluid models.

The acoustic intensity formulation includes the definition of the intensity quantity, the algorithm used to calculate fluid particle velocities using the pressure distribution in a general triangularized domain, and the calculation of the acoustic intensity vector quantity from pressures and velocities. The formulation has been implemented in the program AcINT (Acoustic INTensity), which functions as a post-processor to NASTRAN. An example, a submerged prolate-spheroidal shell with two sets of boundary conditions, is analyzed for a ring load. The resulting acoustic intensity fields are displayed for a given excitation frequency to illustrate the energy flow paths which result. The acoustic intensity vector plots show the utility of the method in identifying dominant power paths in fluid-structure interaction problems.

STRUCTURAL-ACOUSTIC ANALOGY

From an engineering point of view, it is convenient to be able to make use of existing general purpose finite element codes for analyzing structural-acoustic problems. Finite element codes are widely available, versatile, reliable, well supported, and an abundance of pre- and postprocessors may be used with them. Thus we summarize in this section an analogy [34] between the equations of elasticity and the wave equation of acoustics. This analogy allows the coupled structural acoustic problem to be solved with standard finite element codes like NASTRAN.

The pressure p in an acoustic field satisfies the wave equation

$$\nabla^2 p = \frac{\ddot{p}}{c^2}, \tag{1}$$

where ∇^2 is the Laplacian operator, p is the dynamic fluid pressure, c is the wave speed, and dots denote partial differentiation with respect to time.

On the other hand, the x-component of the Navier equations of elasticity, which are the equations solved by structural analysis computer programs, is

$$\frac{\lambda + 2G}{G} u_{,xx} + u_{,yy} + u_{,zz} + \frac{\lambda + G}{G}(v_{,xy} + w_{,xz}) + \frac{1}{G} f_x = \frac{\varrho}{G} \ddot{u}, \tag{2}$$

where u, v, and w are the Cartesian components of displacement, λ is a Lamé elastic constant, G is the shear modulus, f_x is the x-component of body force per unit volume (e.g., gravity), ϱ is the mass density, and commas denote partial differentiation.

A comparison of Eqs. 1 and 2 indicates that elastic finite elements can be used to model scalar pressure fields if we let u, the x-component of displacement, represent p, set $v = w = 0$ everywhere, $f_x = 0$, and $\lambda = -G$. For three-dimensional analysis, the engineering constants consistent with this last requirement are

$$E_e = 10^{20} G_e, \qquad \varrho_e = \frac{G_e}{c^2}, \tag{3}$$

where the element shear modulus G_e can be selected arbitrarily. The subscript "e" has been added to these constants to emphasize that they are merely numbers assigned to the elements.

A variety of boundary conditions may also be imposed. At a pressure-release boundary, $p = 0$ is enforced explicitly like other displacement boundary conditions. For gradient conditions, the pressure gradient $\partial p/\partial n$ is enforced at a boundary point by applying a "force" to the unconstrained DOF at that point equal to $G_e A \partial p/\partial n$, where A is the area assigned to the point and n is the outward normal from the fluid region. For example, the plane wave absorbing boundary condition

$$\frac{\partial p}{\partial n} = -\frac{\dot{p}}{c} \tag{4}$$

is enforced by applying to each point on the outer fluid boundary a "force" given by $-(G_eA/c)\dot{p}$. Since this "force" is proportional to the first time derivative of the fundamental solution variable p, this boundary condition is imposed in the analogy by attaching to the fluid DOF a "dashpot" of constant G_eA/c. The Neumann condition $\partial p/\partial n = 0$ is the natural boundary condition under this analogy. The next higher order local radiation boundary condition, the curved wave absorbing boundary condition [23,36]

$$\frac{\partial p}{\partial n} = -\frac{\dot{p}}{c} - \frac{p}{r}, \tag{5}$$

where r is the radius of the boundary, is enforced under the analogy by attaching in parallel both a "dashpot" and a "spring" between each boundary point and ground.

At a fluid-structure interface (an accelerating boundary), momentum and continuity considerations require that

$$\frac{\partial p}{\partial n} = -\varrho\ddot{u}_n, \tag{6}$$

where n is the normal at the interface, ϱ is the mass density of the fluid, and $\ddot{u}_n$ is the normal component of fluid particle acceleration. Under the analogy, this condition is enforced by applying to the fluid DOF at a fluid-structure interface a "force" given by $-(G_e\varrho A)\ddot{u}_n$.

To summarize, the wave equation, Eq. 1, can be solved with elastic finite elements if the three-dimensional region is modeled with 3-D solid finite elements having material properties given by Eq. 3, and only one of the three Cartesian components of displacement is retained to represent the scalar variable p. In Cartesian coordinates, any of the three components can be used. The solution of axisymmetric problems in cylindrical coordinates follows the same approach except that the z-component of displacement is the only one which can be used to represent p.

FINITE ELEMENT FORMULATION OF FLUID-STRUCTURE INTERACTION

There are two fundamental fluid-structure interaction problems of interest in structural acoustics: acoustic radiation, in which a submerged elastic body is subjected to a mechanical excitation applied to the structure, and scattering, in which the structure is subjected to an external incident pressure loading. For general time-dependent problems, the excitation is an arbitrary function of time, whereas in the time-harmonic case of interest here, the excitation has a single circular frequency ω.

Although our specific interest here is the time-harmonic case, we summarize the theory [22,35] for the more general case, which includes an incident loading as well. The radiation problem will be covered as a special case. For scattering, we assume, without loss of generality, that the incident wave propagates in the negative z direction. The speed of such propagation is c, the speed of sound in the fluid.

Within the fluid region, the total pressure p satisfies the wave equation, Eq. 1. Since the incident free-field pressure p_i is known, it is convenient to decompose the total pressure p into the sum of incident and scattered pressures

$$p = p_i + p_s, \tag{7}$$

each of which satisfies the wave equation.

We now formulate the problem for finite element solution. Consider an arbitrary, submerged, three-dimensional elastic structure subjected to either internal time-dependent loads or an external time-dependent incident pressure. If the structure is modeled with finite elements, the resulting matrix equation of motion for the structural degrees of freedom (DOF) is

$$M\ddot{u} + B\dot{u} + Ku = F - GAp, \tag{8}$$

where M, B, and K are the structural mass, viscous damping, and stiffness matrices (dimension s x s), respectively, u is the displacement vector for all structural DOF (wet and dry) in terms of the coordinate systems selected by the user (s x r), F is the vector of applied mechanical forces applied to the structure (s x r), G is the rectangular transformation matrix of direction cosines to transform a vector of outward normal forces at the wet points to a

vector of forces at all points in the coordinate systems selected by the user (s x f), A is the diagonal area matrix for the wet surface (f x f), p is the vector of total fluid pressures (incident + scattered) applied at the wet grid points (f x r), and dots denote differentiation with respect to time. The pressure p is assumed positive in compression. In the above dimensions, s denotes the total number of independent structural DOF (wet and dry), f denotes the number of fluid DOF (the number of wet points), and r denotes the number of load cases. If first order finite elements are used for the surface discretization, surface areas, normals, and the transformation matrix G can be obtained from the calculation of the load vector resulting from an outwardly directed static unit pressure load on the structure's wet surface. The matrix product GA can then be interpreted as the matrix which converts a vector of negative fluid pressures to structural loads in the global coordinate system. The last two equations can be combined to yield

$$M\ddot{u} + B\dot{u} + Ku + GAp_s = F - GAp_i. \tag{9}$$

A finite element model of the fluid region (with scattered pressure p_s as the unknown) results in a matrix equation of the form

$$Q\ddot{p}_s + C\dot{p}_s + Hp_s = F^{(p)}, \tag{10}$$

where p_s is the vector of scattered fluid pressures at the grid points of the fluid region, Q and H are the fluid "inertia" and "stiffness" matrices (analogous to M and K for structures), C is the "damping" matrix arising from the radiation boundary condition (Eq. 4), and $F^{(p)}$ is the "loading" applied to fluid DOF due to the fluid-structure interface condition, Eq. 6. Using the analogy described in the preceding section, elastic finite elements can be used to model both structural and fluid regions. Material constants assigned to the elastic elements used to model the fluid are specified according to Eq. 3. In three dimensions, elastic solid elements are used (e.g., isoparametric bricks (IHEXi) for general 3-D analysis or solids of revolution (TRIAAX, TRAPAX) for axisymmetric analysis).

At the fluid-structure interface, Eqs. 6 and 7 can be combined to yield

$$\frac{\partial p_s}{\partial n} = \varrho(\ddot{u}_{ni} - \ddot{u}_n), \tag{11}$$

where n is the outward unit normal, and $\ddot{u}_{ni}$ and $\ddot{u}_n$ are, respectively, the incident and total outward normal components of fluid particle acceleration at the interface. Thus, from the analogy, we impose the fluid-structure interface condition by applying a "load" to each interface fluid point given by

$$F^{(p)} = -\varrho G_e A(\ddot{u}_{ni} - \ddot{u}_n), \tag{12}$$

where the first minus sign is introduced since, in the coupled problem, we choose n as the outward normal from the structure into the fluid, making n an inward normal for the fluid region. The normal displacements u_n are related to the total displacements u by the same rectangular transformation matrix G used above:

$$u_n = G^T u, \tag{13}$$

where the superscript T denotes the matrix transpose. Eqs. 10, 12, and 13 can be combined to yield

$$Q\ddot{p}_s + C\dot{p}_s + Hp_s - \varrho G_e(GA)^T\ddot{u} = -\varrho G_e A\ddot{u}_{ni}. \tag{14}$$

Since the fluid-structure coupling terms in Eqs. 9 and 14 are nonsymmetric, we symmetrize the problem [21] by using a new fluid unknown q such that

$$q = \int_0^t p_s dt, \qquad \dot{q} = p_s. \tag{15}$$

If Eq. 14 is integrated in time, and the fluid element "shear modulus" G_e is chosen as

$$G_e = \frac{-1}{\varrho}, \tag{16}$$

the overall matrix system describing the coupled problem can be written as

$$\begin{bmatrix} M & 0 \\ 0 & Q \end{bmatrix} \begin{Bmatrix} \ddot{u} \\ \ddot{q} \end{Bmatrix} + \begin{bmatrix} B & (GA) \\ (GA)^T & C \end{bmatrix} \begin{Bmatrix} \dot{u} \\ \dot{q} \end{Bmatrix} + \begin{bmatrix} K & 0 \\ 0 & H \end{bmatrix} \begin{Bmatrix} u \\ q \end{Bmatrix} = \begin{Bmatrix} F - (GA)p_i \\ Av_{ni} \end{Bmatrix}, \tag{17}$$

where v_{ni} $(= u_{ni})$ is the outward normal component of incident fluid particle velocity.

The new variable q is, except for a multiplicative constant, the velocity potential ϕ, since

$$p = -\varrho\dot{\phi}. \tag{18}$$

Eq. 17 could also be recast in terms of ϕ rather than q as the fundamental fluid unknown, but no particular advantage would result. In fact, the use of q rather than ϕ has the practical advantage that the fluid pressure can be recovered directly from the finite element program as the time derivative (velocity) of the unknown q.

To summarize, both structural and fluid regions are modeled with finite elements. For the fluid region, the material constants assigned to the finite elements are

$$E_e = \frac{-10^{20}}{\varrho}, \quad G_e = \frac{-1}{\varrho}, \quad \nu_e = \text{unspecified}, \quad \varrho_e = \frac{-1}{\varrho c^2}, \tag{19}$$

where E_e, G_e, ν_e, and ϱ_e are the Young's modulus, shear modulus, Poisson's ratio, and mass density, respectively, assigned to the fluid finite elements. The properties ϱ and c above are the actual density and sound speed for the fluid medium. The radiation boundary condition used is the plane wave approximation, Eq. 4, which appears to be adequate if the outer fluid boundary is sufficiently far from the structure [20]. With this boundary condition, matrix C in Eq. 17 arises from dashpots applied at the outer fluid boundary with damping constant $-A/(\varrho c)$ at each grid point to which the area A has been assigned. At the fluid-structure interface, matrix GA is entered using the areas (or areal direction cosines) assigned to each wet degree of freedom. (Recall that GA can be interpreted as the matrix which converts a vector of negative fluid pressures to structural loads in the global coordinate system.)

For radiation problems, the right-hand side of Eq. 17 can be simplified further since the incident pressure p_i is zero, and we obtain

$$\begin{bmatrix} M & 0 \\ 0 & Q \end{bmatrix} \begin{Bmatrix} \ddot{u} \\ \ddot{q} \end{Bmatrix} + \begin{bmatrix} B & (GA) \\ (GA)^T & C \end{bmatrix} \begin{Bmatrix} \dot{u} \\ \dot{q} \end{Bmatrix} + \begin{bmatrix} K & 0 \\ 0 & H \end{bmatrix} \begin{Bmatrix} u \\ q \end{Bmatrix} = \begin{Bmatrix} F \\ 0 \end{Bmatrix}. \tag{20}$$

We note that the structural and fluid unknowns are not sequenced as perhaps implied by the partitioned form of Eq. 20. The coupling matrix GA is quite sparse and has nonzeros only for matrix rows associated with the structural DOF at the fluid-structure interface and columns associated with the coincident fluid points. Thus, the grid points should be sequenced for minimum matrix bandwidth or profile as if the structural and fluid meshes comprised a single large mesh. As a result, the structural and fluid grid points will, in general, be interspersed in their numbering, and the system matrices will be sparse and banded.

ACOUSTIC INTENSITY CALCULATIONS

The procedure for solving for the acoustic intensity field in an axisymmetric fluid finite element model using NASTRAN [33] and the acoustic intensity post-processor AcINT is:

- run NASTRAN on a dynamically loaded finite element model of structural elements and fluid elements using direct frequency response analysis, and generate resultant nodal pressures for the fluid region(s);
- run AcINT using the output from NASTRAN to calculate nodal fluid velocities and acoustic intensities.

The nodal pressures, actually the cosine coefficients of nodal pressures, are computed by NASTRAN in response to the AXISYMMETRIC = COSINE command in the case control part of the input data. Since only cosine coefficients are requested, the 2, 4, and 6 DOF are removed by NASTRAN for harmonic zero. The 1 and 5 DOF must be constrained by the user, leaving the 3 DOF to represent the scalar fluid velocity potential.

The velocity potential integrated over time is the fluid pressure. Therefore, in the analogy, nodal pressures are obtained by the case control command VELOCITY = ALL (or SETID). The resultant fluid nodal pressures are used as illustrated below to compute acoustic velocities and intensities.

Acoustic Intensity

Intensity is defined as the time averaged product of a pressure with the in-phase component of particle velocity. For time-harmonic analysis, where complex numbers are used, this calculation may be visualized as taking the dot product of the pressure and velocity phasors. Multiplying one complex number by the in-phase part of another complex number is the same operation as multiplying the first number by the complex conjugate of the other number and taking the real part of the result:

$$\vec{I} = \Re\,[p\vec{v}^{*}], \tag{21}$$

where p is pressure, and $\vec{v}^{*}$ is the complex conjugate of velocity. (Often, a factor of 1/2 appears in intensity equations. However there is no factor 1/2 in the equations if the assumption is made that pressures and velocities are "effective" rms values rather than amplitudes. With this assumption, consistency is maintained, and there is no mixing of effective and peak quantities in this formulation.)

Acoustic Velocities

The derivation of acoustic velocities for axisymmetric problems is performed for the cosine coefficients of the Fourier summation about the axis of rotational symmetry (z), where the r, z, and rotation about θ DOF are active. Only the r and z variations of the scalar pressure field are used to calculate the acoustic velocity vector field. The particle velocity in a fluid domain is defined as:

$$\vec{v} = \frac{i}{\omega\varrho}\nabla p = \frac{i}{\omega\varrho}\left(\frac{\partial p}{\partial r}\hat{i} + \frac{\partial p}{\partial z}\hat{k}\right), \tag{22}$$

where ϱ is the fluid density, ω is the circular frequency, i is the square root of -1, $\frac{\partial p}{\partial r}$ and $\frac{\partial p}{\partial z}$ are the pressure derivatives in the r and z directions, and $\hat{i}$ and $\hat{k}$ are unit vectors in the r and z directions, respectively. A first order finite difference approximation of the pressure derivatives at the nodes in an individual TRIAAX element can be made as shown in Figure 1. The pressure differences between nodes are divided by the distances between nodes to approximate the first derivative of pressure in the direction of the two nodes. The approximate pressure

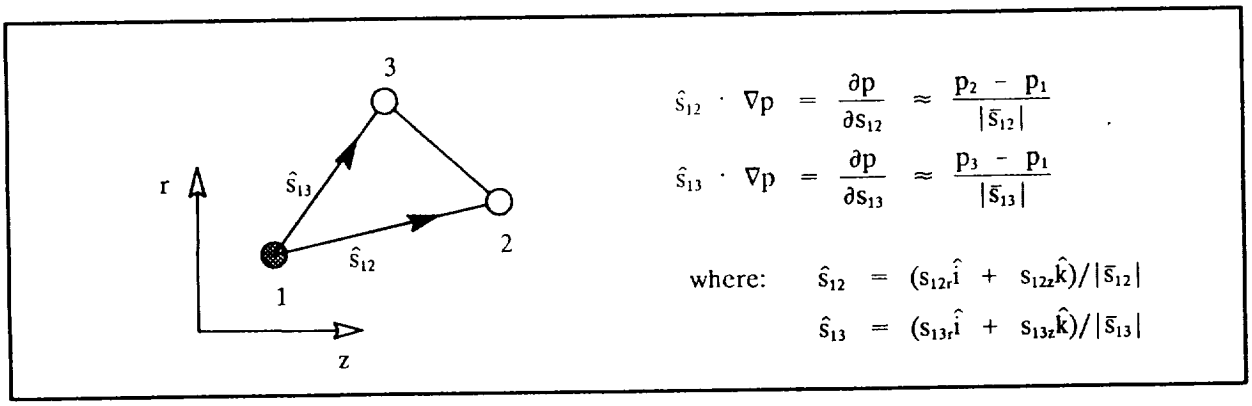

Figure 1. Pressure Gradient Approximation.

gradient equations are written for all nodes connected to the node for which the velocity vector is to be calculated. In the case above, all elements connected to node 1 must be found, and equations are written for each node connected to node 1. No duplicate equations are written when two elements share a common edge. An overdetermined system of equations for the pressure derivatives in the r and z directions is the result, with one

equation for each node connected to the primary node. The system of equations is

$$\begin{bmatrix} s_{1r} & s_{1z} \\ s_{2r} & s_{2z} \\ \cdot & \cdot \\ \cdot & \cdot \\ \cdot & \cdot \\ s_{Nr} & s_{Nz} \end{bmatrix} \begin{Bmatrix} \frac{\partial p}{\partial r} \\ \frac{\partial p}{\partial z} \end{Bmatrix} = \begin{Bmatrix} \frac{\partial p}{\partial s_1} \\ \frac{\partial p}{\partial s_2} \\ \cdot \\ \cdot \\ \cdot \\ \frac{\partial p}{\partial s_N} \end{Bmatrix} \tag{23}$$

where s_{ir} and s_{iz} are the r and z components of the unit vector from the primary node to the connecting node i, and N is the number of connecting nodes.

The derivatives are determined approximately using a least squares approach. The particle velocity vector is then solved for using Equation 22, and the acoustic intensity vector is given by Equation 21. The axisymmetric acoustic intensity field for a complete domain is found by repeating this procedure for each node in the domain. In this way, a complete energy flow solution can be derived from nodal pressures and element connectivities.

EXAMPLES

The axisymmetric model of a submerged, half prolate spheroidal shell is shown in Figure 2. The structure has a semi axes of 10 m and 5 m. The material is steel with a uniform thickness of 25 mm, a Young's modulus (E) of 2.074 E11 N/m^2, a density (ρ) of 7860 kg/m^3, a Poisson's ratio (ν) of 0.3, and a material loss factor of 0.0. The frequency range of interest was 100 to 500 Hz. The problem was analyzed for harmonic zero, commonly referred to as the "breathing mode" of the domain, implying no variation in the solution field about the z axis.

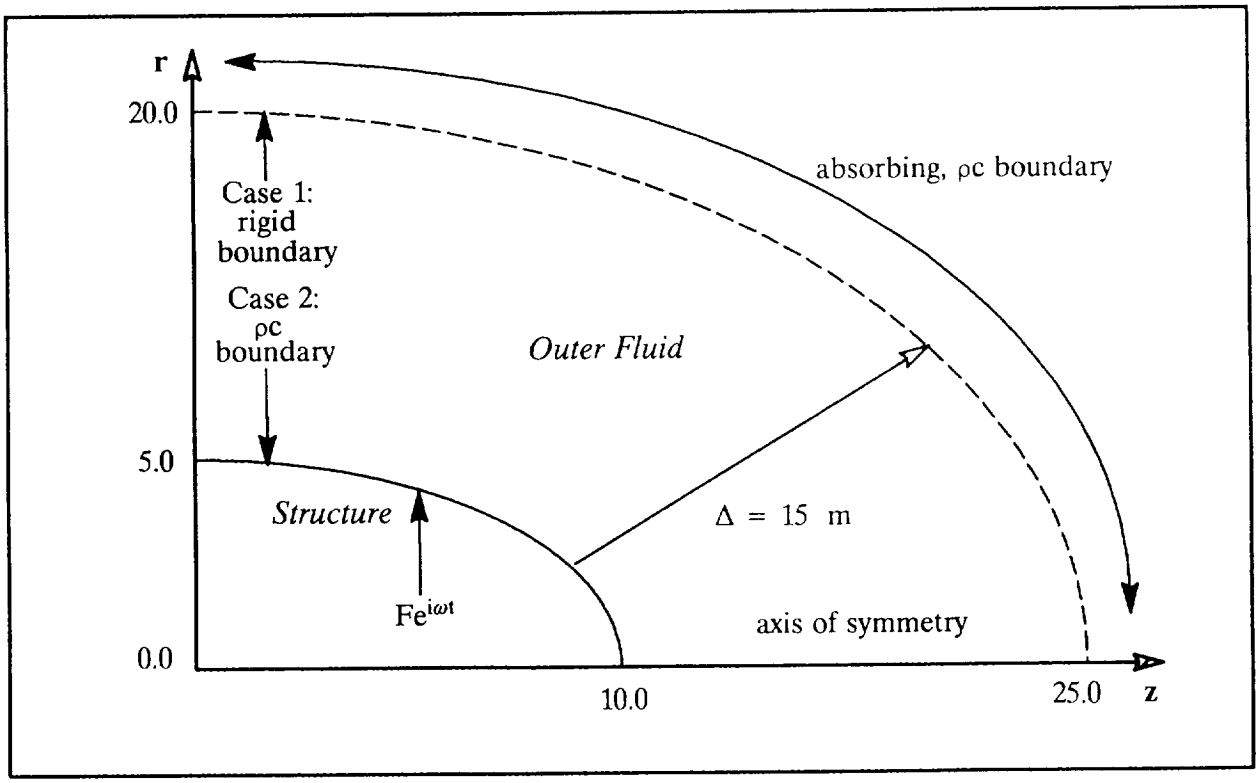

Figure 2. Axisymmetric Model of a Submerged, Half Prolate-spheroid.

As shown in the diagram, the structure is submerged in fluid, which was also modeled and interfaced with the structure. The fluid is seawater, with a density (ρ) of 1025 kg/m^3 and a speed of sound (c) of 1500 m/s. Two sets of boundary conditions along the left, vertical fluid edge were applied, and are discussed in more detail below.

A finite element (CONEAX) model of the problem is shown in Figure 3. The structure was modeled using axisymmetric conical shell elements. The plate thickness, steel material properties, and the frequency range determine an estimated average flexural wavelength [38] of 0.7 m at 500 Hz, which for a mesh requirement of about eight elements/wavelength translates to a structural mesh density of 0.087 m/element length.

The outer fluid was modeled using TRIAAX elements. The seawater properties and frequency range determine an upper wavelength of 15.0 m and a lower wavelength of 3.0 m. The upper wavelength determines the location of the outer boundary of the fluid mesh, shown as Δ in Figure 2, as one wavelength from the structure, or 15.0 m. The lower wavelength determines the fluid mesh density, which for a minimum of 8 elements/wavelength, specifies a fluid mesh size of 0.375 m/element length. The fluid and structural meshes are distinct at the fluid-structure boundary, but with coincident nodes. These coincident nodes are coupled by area matrices which map fluid pressures to structural forces, as described earlier. Only one fluid DOF was assigned to each mesh point.

The area matrices are input with DMIG cards, which apply area values to the damping, or B2PP matrix. A current limitation of NASTRAN is the program performing nonsymmetric system matrix decompositions when MPC data is used with DMIG input. Despite the DMIG input being declared symmetric, when the MPC equations are used to obtain the BDD matrix, NASTRAN changes the matrix trailer to nonsymmetric. All matrix operations become nonsymmetric as a result, greatly increasing computer time. A sequence of ALTER statements may be used to restore the trailer to its symmetric form. One such sequence (for the 1990 version of NASTRAN, Rigid Format 8) is shown below for BDD.

```
ALTER 119$                          Make BDD trailer symmetric
DIAGONAL BDD/AVEC/*COLUMN*/0.$      Vector of ones
ADD AVEC,/PVEC/(0.0,0.0)$           Vector of zeros (P-Vec)
MERGE BDD,,,,PVEC,/BDDSYM/-1//6$    Dummy merge
EQUIV BDDSYM,BDD$                   BDD now symmetric
```

This alter is inserted before the FRRD module. With the BDD symmetry flag restored, subsequent matrix operations will take advantage of the symmetry of the system, reducing the required computer time. This NASTRAN bug has been fixed by Gordon Chan of Unisys for the 1992 program release.

Since the structural elements are about one-quarter the size of the desired fluid elements, some mesh transitioning in the fluid meshes was required from the mesh density of the structure (0.087 m/element length) to the mesh density of the fluid (0.375 m/element length). The fluid element material properties were assigned according to Eq. 19.

Boundary and Loading Conditions

Two sets of boundary conditions were applied in the problem. In both cases, a ρc impedance, or plane wave absorbing boundary condition was applied to the curved outer fluid boundary; and a point forcing function was applied at $z = 6.0$ in the positive r direction along the structure, as shown in Figure 2. The structure was constrained in all degrees of freedom at the upper left end. The left vertical fluid boundary was modeled in two ways: (1) as a rigid wall, which reflects incident waves, and (2) as a ρc impedance absorber. DMIG statements inputting $-A/\rho c$ values for all boundary points simulated the ρc plane wave absorber.

Results

The problem may be accurately solved for any set of frequencies from 100 to 500 Hz. Detailed results are presented here for the 100 Hz case for Cases 1 and 2. The numerical output is examined several ways: power input and power radiation calculations, structural displacements, acoustic pressure contour plots, and acoustic intensity vector plots. This set of output provides a nearly complete solution to the structural-acoustic problem.

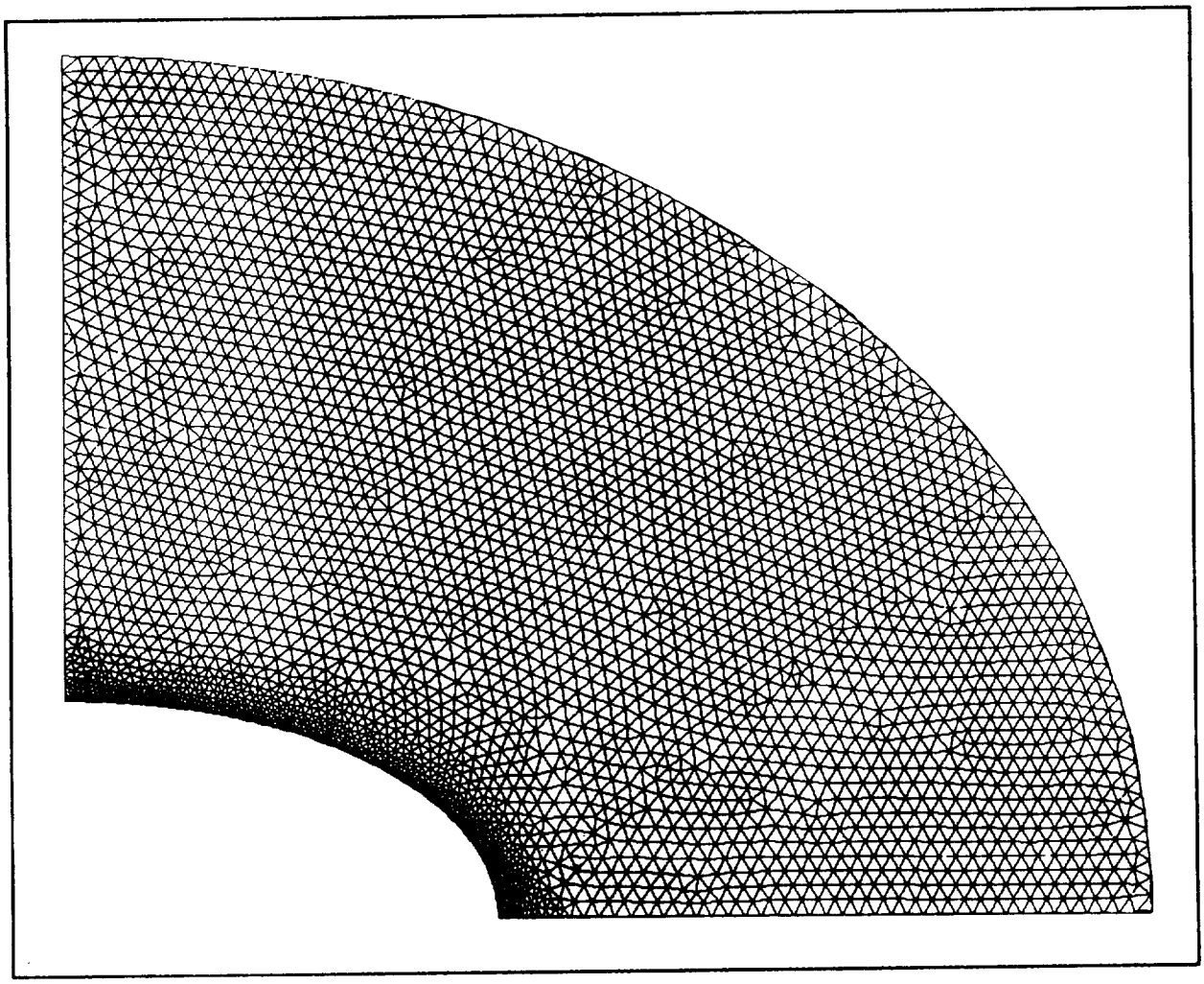

Figure 3. Finite Element Mesh.

Since both materials are lossless, all power entering the structure must eventually be radiated into the fluid. This means the power input by the forcing function must equal the power exiting the system through the plane-wave absorbing outer boundaries. Power input is defined as

$$P_{in} = F_{in} v_{in}^{*} \tag{24}$$

where F_{in} is the radial complex input force (in this case unity), and v_{in}^{*} is the complex conjugate of the corresponding velocity at the force point. The power radiated through the absorbing boundary may be found by integrating the calculated acoustic intensity field normal to the boundary:

$$P_{rad} = \int_{C} \vec{I} \cdot \hat{n} \, dA, \tag{25}$$

where C denotes the boundary contour, $\hat{n}$ is the outward normal vector, and dA is the incremental area. This integration may be converted to a summation over all nodes on the boundary, where

$$P_{rad} = \sum_{i=1}^{n} \vec{I}_i \cdot \hat{n}_i \, A_i. \tag{26}$$

In this case, $\hat{n}_i$ and A_i are calculated for each node on the boundary, and used with the intensity vector at each node to calculate the power leaving the system. The summation over all boundary nodes gives the total radiated power.

Radiated power is commonly represented by a spherical pressure field with a reference radius of one yard. If the outer boundary is in the far-field, the pressure at one yard is

$$p_{1yard}(dB) = 20\log\sqrt{\frac{\varrho c P_{rad}}{2\pi r^2}} + 120, \quad (27)$$

where 120 dB is added to calculate the pressure relative to 1 μPa.

Table1 lists the power quantities defined above, and the relative error calculated by subtracting the radiated power from the input power and normalizing to the input power. The error, about 2% for each case, is probably due to the curved outer boundary. The approximate boundary condition was of a plane-wave absorbing boundary. Since neither the boundary nor the radiated waves is perfectly plane, small reflections at the boundary can occur, causing the power balance to be slightly in error. The radiated power, and therefore the pressure at 1 yard, is higher for Case 2, and the error is either due to the additional left ϱc boundary's absorbing more power, or the boundary's causing a small shift in the frequency response of the system. A full frequency sweep would be required to determine the effects of the left absorbing boundary.

Case	Power Input (W)	Power Radiated (W)	%Error	Pressure@1 yard (dB re: 1 μPa)
1	1.499E-8	1.519E-8	-1.33	91.9
2	8.988E-8	8.798E-8	2.11	99.5

Table1. Power Results for 100 Hz.

A plot of the displaced shapes of the structure for both cases is shown in Figure 4. The displacement field of the structure is complex, and a time dependent animation of the structural response is required to visualize fully the movement. The plots shown here are at a single phase angle in the displacement cycle (292.5°), and show that the change in boundary condition does not significantly alter the structural response. A small phase shift has occurred, but the general shape is the same for both cases. The ring loading causes the discontinuity in the waveform at z = 6.0. This point is the source of the waves travelling to the left and right from the load.

Acoustic intensity vector plots are superimposed on acoustic pressure contour plots in Figures 5-8. Figure 5 shows the entire field for Case 1, and Figure 6 is a close-up of the field near the structure. Figure 7 is a plot representing Case 2, and Figure 8 is a closer view. A common pressure scale is used for all plots, with the letters on the contours corresponding to the pressure levels (dB re: 1 μPa). The vector lengths are proportional to the log of the intensity magnitudes. The log of intensity is used in the plots to overcome the 1/r decay in intensity magnitude with distance. Since this is an axisymmetric analysis at circumferential harmonic zero, the acoustic fields are constant for all angles about the z axis, and no net energy may pass through the lower z boundary. All intensity vectors along the lower boundary therefore have zero radial components.

The plots for Case 1 (Figure 5 and Figure 6) show the highest levels of far-field pressures to be in the r and z directions, with values between contours I and J, or 70 to 75 dB. Near-field pressure peaks are indicated near the structure by D contours, or about 100 dB levels. Examining the far-field intensity vectors show a far-field condition (all acoustic energy directed outward) at the outer boundary, with the dominant energy flow paths in the r and z directions. The rigid boundary condition along the left wall is evidenced by the absence of any outward z directed intensity component along it. The near-field intensity vectors shows an energy path that begins at the load point (z = 6.0) and branches to the right and left. At the right, or bottom of the structure, energy flows along the fluid-structure boundary before travelling away toward the far-field at the r = 0 boundary. To the left of the load point, energy re-enters and re-exits the structure twice before radiating outward at the z = 0 boundary. The circulation of power to the left of the load point causes "false sources" to appear where the energy re-exits the structure. Examination of the entire intensity field identifies the load point as the original source of power though.

For Case 2, the use of the ϱc boundary (Figure 7 and Figure 8) and at the left edge of the fluid causes the acoustic pressures in the r direction, or upper left of the fluid domain, to decrease significantly from the rigid boundary case, from 75 to 55 dB. The acoustic intensity field shows the reason for the decrease in pressure; the

vectors along the ρc boundary now have a z-directed component, implying power exiting the system through the boundary. The overall radiated power is higher for Case 2, though, due to an increase in the radiated energy along the midsection of the outer boundary. The near-field intensity plot reveals that the circulating power flows between structure and fluid to the left of the load point have disappeared. The energy now flows along the fluid-structure boundary and radiates outward at the top of the structure. To the right of the load however, power now circulates. The dominant path is from the load point to the right; into and out of the structure; then along the structure until r = 0, where some power reenters the structure, and the rest radiates outward along the z axis.

NASTRAN DIFFICULTIES ENCOUNTERED

Two important limitations of NASTRAN became apparant during this study: the BDD damping matrix's being specified as unsymmetric regardless of the symmetric nature of fluid structure interaction and absorbing boundary data input by DMIG cards; and the formulation of stiffness coefficients for CONEAX elements. The BDD matrix trailer may be restored to symmetric using the ALTER statements outlined in the Example section. The difficulties with the CONEAX formulation are not easily fixed however.

Stiffnesses for CONEAX elements are computed analytically by NASTRAN, and involve the inverse of $\Delta r/\Delta l$, where Δr is the difference in radii and Δl is the total distance between the grids defining an element. For perfectly cylindrical shell elements with no variation in radii ($\Delta r/\Delta l = 0$), a different formulation is used to avoid a floating point error caused by a division by zero. However, no provision is made for small relative variation in radii ($\Delta r/\Delta l \approx 0$), and for a small range of elements the analytical computation is corrupted when computer precision limits are reached. Sometimes the error is so drastic that negative values are obtained for self term (diagonal) stiffnesses. The negative stiffnesses are reported to the user when NASTRAN checks the system matrices for singularities. However, sometimes the error may be drastic in the positive sense, i.e., stiffnesses orders of magnitude too large. No error would be reported to the user, and the final solution would be incorrect.

CONEAX stiffness errors were encountered for the example described here at the upper left end of the structure, where the elements become nearly cylindrical. In this case, the stiffnesses of several of the near cylindrical elements were output and analyzed for accuracy. The two end elements were found to have large errors in stiffness. To solve the problem, the radii of the element grid points were set equal, and the end of the structure was approximated as purely cylindrical.

A possible programming solution to the sensitivity of CONEAX stiffnesses to small relative differences in radii is to approximate nearly cylindrical regions as cylindrical. For example, if for a given element $\Delta r/\Delta l$ is below some specified tolerance ϵ, the second grid radius is set equal to the first grid radius. The resulting model would be a stepwise approximation of the nearly cylindrical region. The chief problem is how to choose ϵ. Studies would have to be performed on ranges of nearly cylindrical elements using different levels of computer precision to determine the accuracy limits on the analytical stiffness computation method.

CONCLUSIONS

The combination of structural displacement plots, pressure contours, and acoustic intensity vector fields all serve to reveal the complete state of a structural-acoustic problem. However, one component of the response is missing: the energy flow within the structure. The circulating energy along the structural-acoustic boundary indicated by the intensity plots show power flowing through the structure. A formulation similar to that for acoustic intensity can be performed for the structure; however more than one wave type must be considered. For the axisymmetric shells of revolution (CONEAX) used here, for example, both flexural (composed of both shear and moment waves) and longitudinal waveforms may transport energy through structures. Methods have been developed for general three-dimensional structural models of beams (BAR) and plates (QUAD4) [39], but have not yet been extended to axisymmetric problems. This additional analysis tool will help improve considerably the understanding of structural-acoustic, frequency response problems.

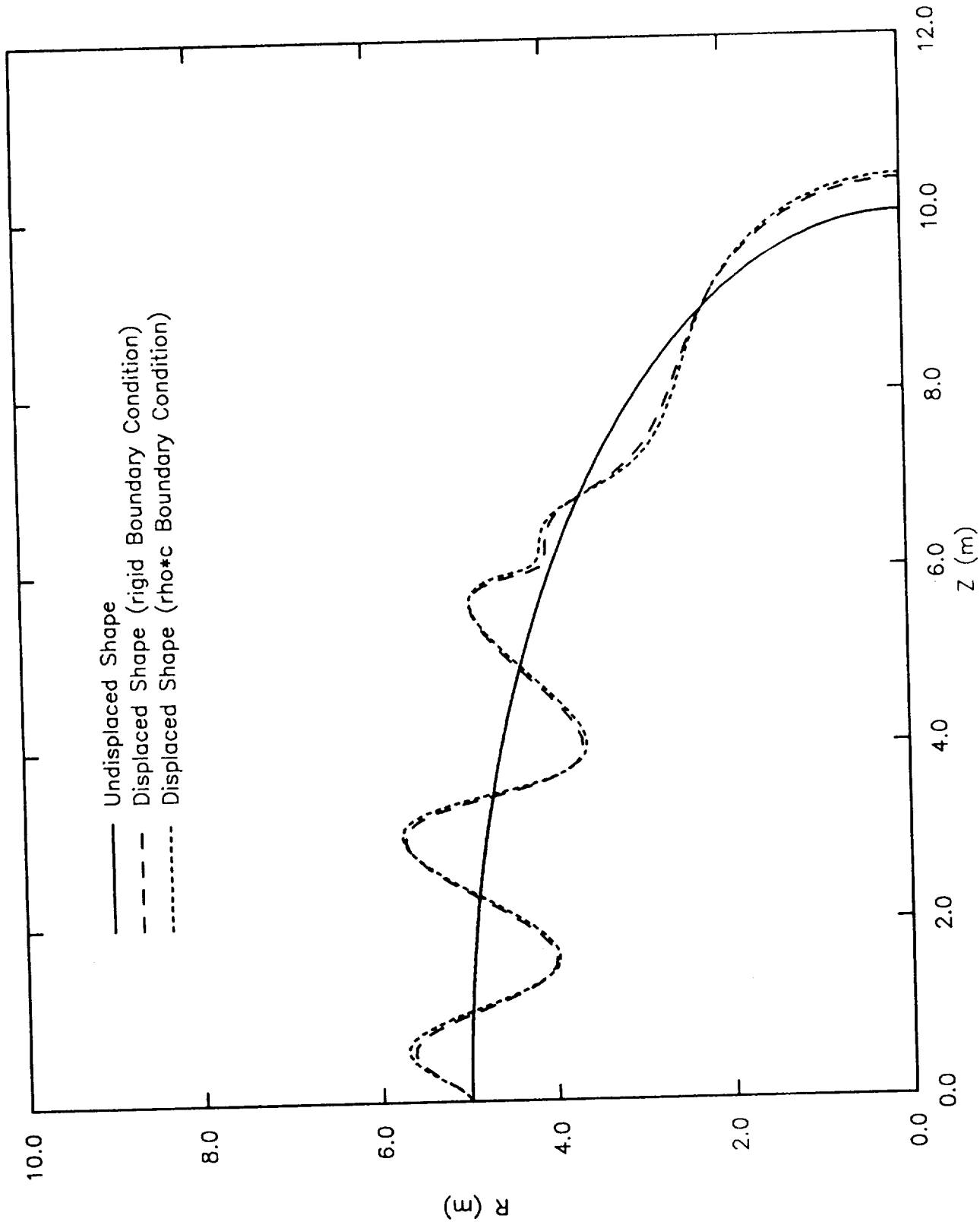

Figure 4. Structural Displacements for both Boundary Condition Cases (phase = 292.5°).

Figure 5. Acoustic Intensities and Pressures for Rigid Vertical Boundary; Lines Denote Constant Pressure Contours; Vectors Denote Acoustic Intensities.

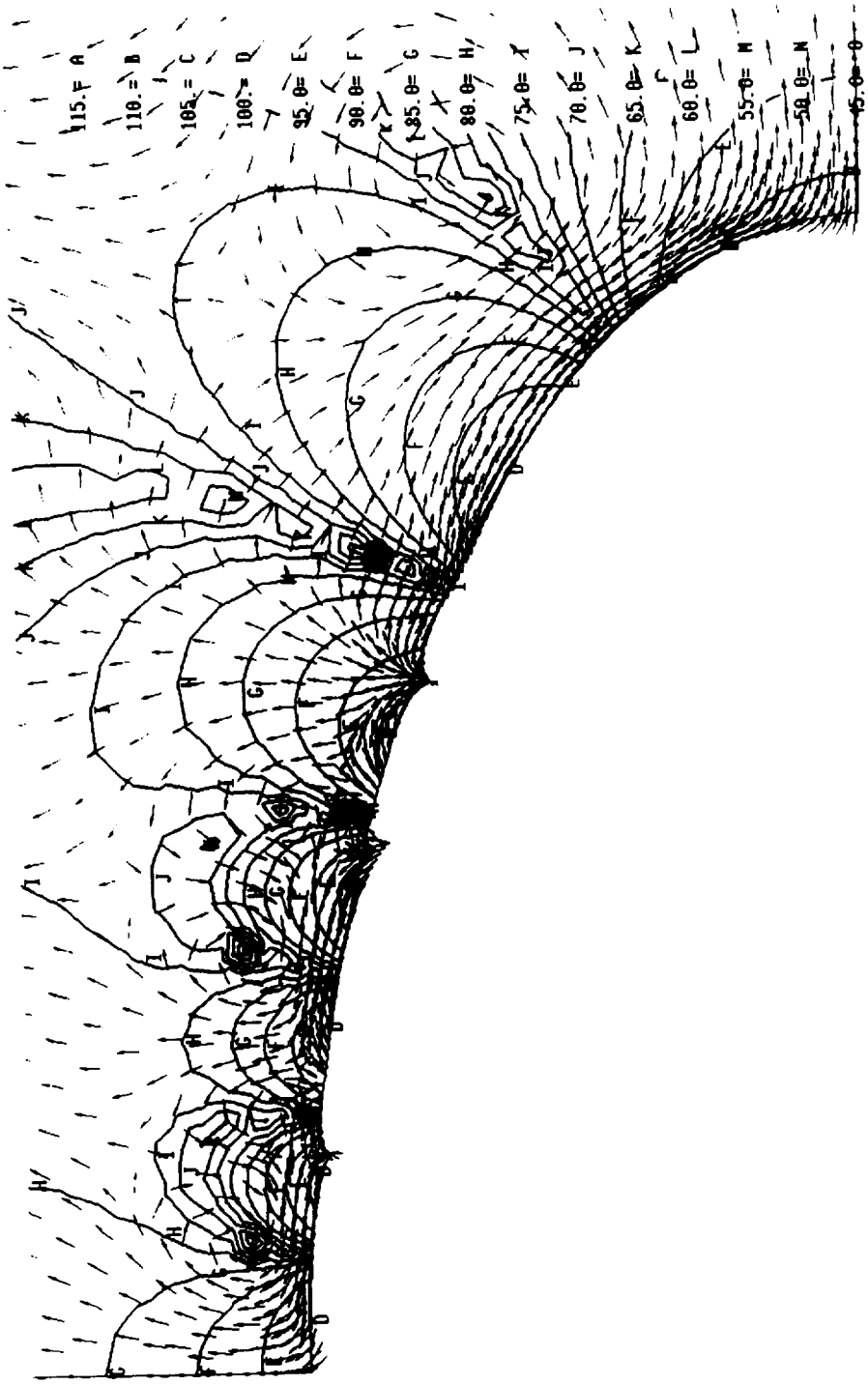

Figure 6. Close-up of Acoustic Intensities and Pressures for Rigid Vertical Boundary; Lines Denote Constant Pressure Contours; Vectors Denote Acoustic Intensities.

C-3

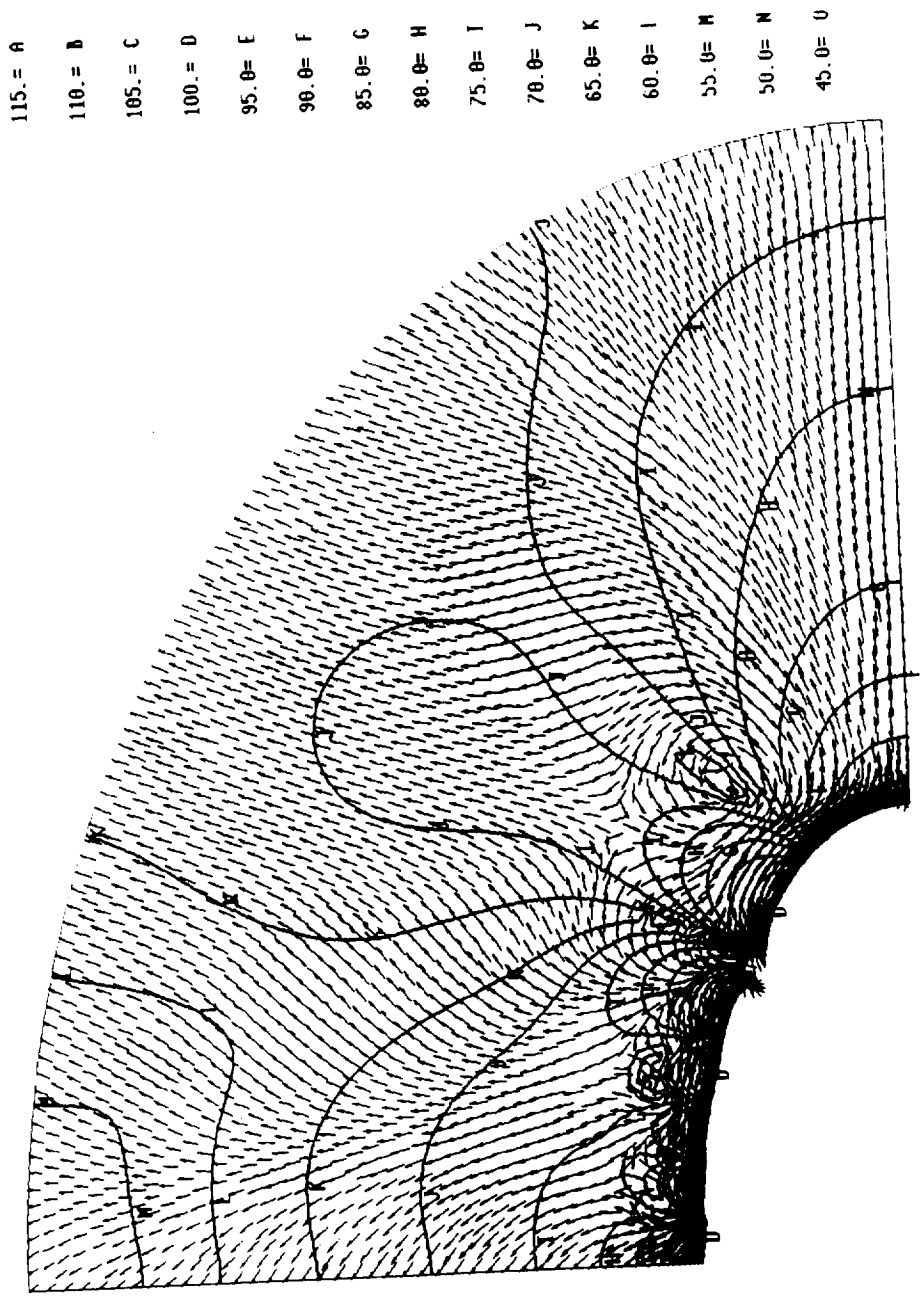

Figure 7. Acoustic Intensities and Pressures for Absorbing Vertical Boundary; Lines Denote Constant Pressure Contours; Vectors Denote Acoustic Intensities.

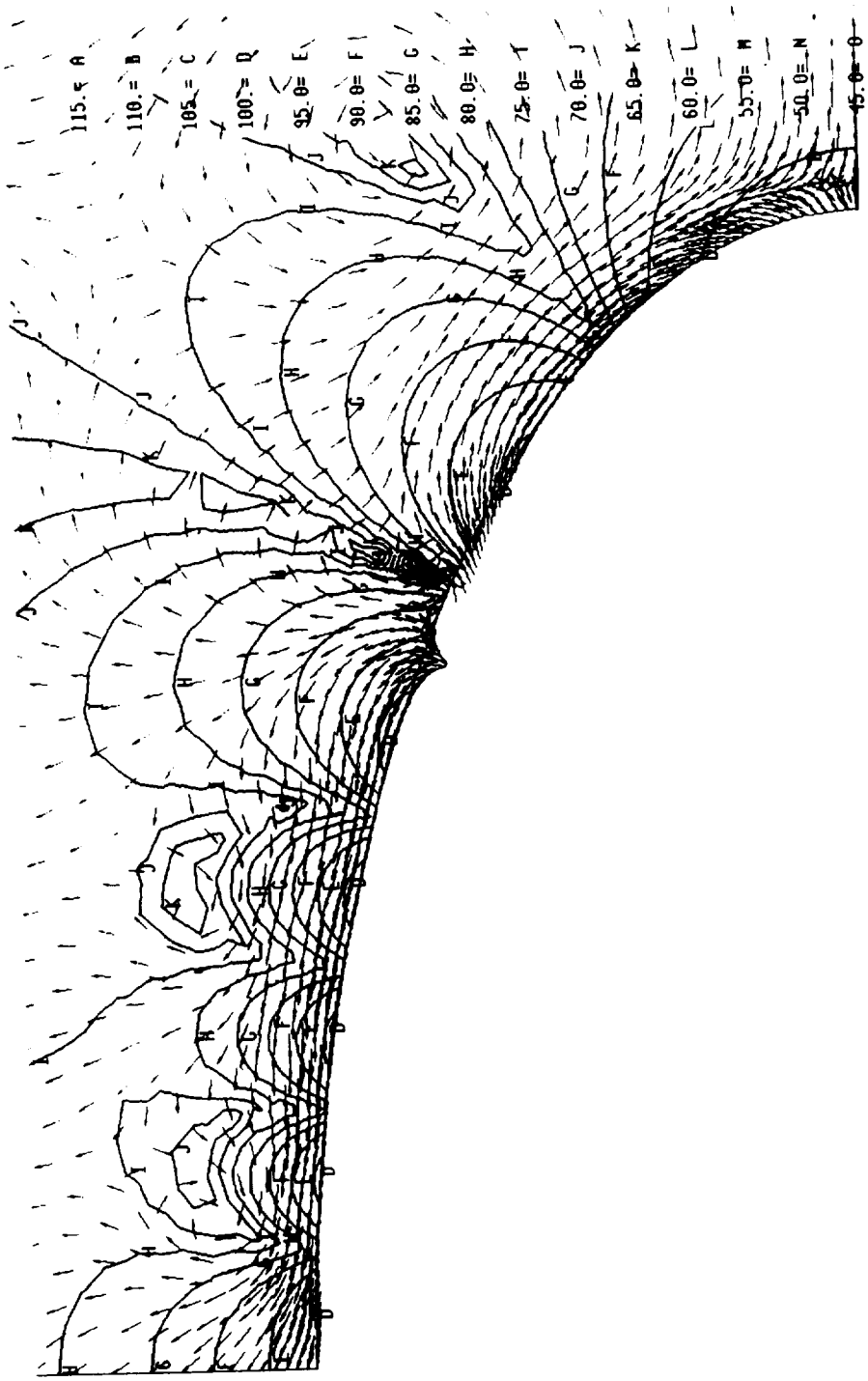

Figure 8. Close-up of Acoustic Intensities and Pressures for Absorbing Vertical Boundary; Lines Denote Constant Pressure Contours; Vectors Denote Acoustic Intensities.

REFERENCES

1. L.H. Chen and D.G. Schweikert, "Sound Radiation from an Arbitrary Body," *J. Acoust. Soc. Amer.*, Vol. 35, No. 10, pp. 1626-1632 (1963).

2. J.J. Engblom and R.B. Nelson, "Consistent Formulation of Sound Radiation from Arbitrary Structure," *J. Appl. Mech.*, Vol. 42, pp. 295-300 (1975).

3. H. Huang, G.C. Everstine, and Y.F. Wang, "Retarded Potential Techniques for the Analysis of Submerged Structures Impinged by Weak Shock Waves," *Computational Methods for Fluid-Structure Interaction Problems*, ed. by T. Belytschko and T.L. Geers, AMD-Vol. 26, The American Society of Mechanical Engineers, New York, pp. 83-93 (1977).

4. D.T. Wilton, "Acoustic Radiation and Scattering from Elastic Structures," *Int. J. Num. Meth. in Engrg.*, Vol. 13, pp. 123-138 (1978).

5. J.S. Patel, "Radiation and Scattering from an Arbitrary Elastic Structure Using Consistent Fluid Structure Formulation," *Comput. Struct.*, Vol. 9, pp. 287-291 (1978).

6. Y.P. Lu, "The Application of Retarded Potential Techniques to Submerged Dynamic Structural Systems," *Innovative Numerical Analysis for the Engineering Sciences*, edited by R. Shaw, W. Pilkey, B. Pilkey, R. Wilson, A. Lakis, A. Chaudouet, and C. Marino, University Press of Virginia, Charlottesville (1980).

7. I.C. Mathews, "Numerical Techniques for Three-Dimensional Steady-State Fluid-Structure Interaction," *J. Acoust. Soc. Amer.*, Vol. 79, pp. 1317-1325 (1986).

8. G.C. Everstine, F.M. Henderson, E.A. Schroeder, and R.R. Lipman, "A General Low Frequency Acoustic Radiation Capability for NASTRAN," *Fourteenth NASTRAN Users' Colloquium*, NASA CP-2419, National Aeronautics and Space Administration, Washington, DC, pp. 293-310 (1986).

9. G.C. Everstine, F.M. Henderson, and L.S. Schuetz, "Coupled NASTRAN/Boundary Element Formulation for Acoustic Scattering," *Fifteenth NASTRAN Users' Colloquium*, NASA CP-2481, National Aeronautics and Space Administration, Washington, DC, pp. 250-265 (1987).

10. A.F. Seybert, T.W. Wu, and X.F. Wu, "Radiation and Scattering of Acoustic Waves from Elastic Solids and Shells Using the Boundary Element Method," *J. Acoust. Soc. Amer.*, Vol. 84, pp. 1906-1912 (1988).

11. G.C. Everstine and F.M. Henderson, "Coupled Finite Element/Boundary Element Approach for Fluid-Structure Interaction," *J. Acoust. Soc. Amer.*, Vol. 87, No. 5, pp. 1938-1947 (1990).

12. O.C. Zienkiewicz and R.E. Newton, "Coupled Vibrations of a Structure Submerged in a Compressible Fluid," *Proc. Internat. Symp. on Finite Element Techniques*, Stuttgart, pp. 359-379 (1969).

13. A. Craggs, "The Transient Response of a Coupled Plate-Acoustic System Using Plate and Acoustic Finite Elements," *J. Sound and Vibration*, Vol. 15, No. 4, pp. 509-528 (1971).

14. A.J. Kalinowski, "Fluid Structure Interaction," *Shock and Vibration Computer Programs: Reviews and Summaries*, SVM-10, ed. by W. Pilkey and B. Pilkey, The Shock and Vibration Information Center, Naval Research Laboratory, Washington, DC, pp. 405-452 (1975).

15. L. Kiefling and G.C. Feng, "Fluid-Structure Finite Element Vibrational Analysis," *AIAA J.*, Vol. 14, No. 2, pp. 199-203 (1976).

16. A.J. Kalinowski, "Transmission of Shock Waves into Submerged Fluid Filled Vessels," *Fluid Structure Interaction Phenomena in Pressure Vessel and Piping Systems*, PVP-PB-026, ed. by M.K. Au-Yang and S.J. Brown, Jr., The American Society of Mechanical Engineers, New York, pp. 83-105 (1977).

17. O.C. Zienkiewicz and P. Bettess, "Fluid-Structure Dynamic Interaction and Wave Forces: An Introduction to Numerical Treatment," *Int. J. Num. Meth. in Engrg.*, Vol. 13, No. 1, pp. 1-6 (1978).

18. M.A. Hamdi and Y. Ousset, "A Displacement Method for the Analysis of Vibrations of Coupled Fluid-Structure Systems," *Int. J. Num. Meth. in Engrg.*, Vol. 13, No. 1, pp. 139-150 (1978).

19. R.E. Newton, "Finite Element Study of Shock Induced Cavitation," Preprint 80-110, American Society of Civil Engineers, New York (1980).

20. A.J. Kalinowski and C.W. Nebelung, "Media-Structure Interaction Computations Employing Frequency-Dependent Mesh Size with the Finite Element Method," *Shock Vib. Bull.*, Vol 51, No. 1, pp. 173-193 (1981).

21. G.C. Everstine, "A Symmetric Potential Formulation for Fluid-Structure Interaction," *J. Sound and Vibration*, Vol. 79, pp. 157-160 (1981).

22. G.C. Everstine, "Structural-Acoustic Finite Element Analysis, with Application to Scattering," in *Proc. 6th Invitational Symposium on the Unification of Finite Elements, Finite Differences, and Calculus of Variations*, edited by H. Kardestuncer, Univ. of Connecticut, Storrs, Connecticut, pp. 101-122 (1982).

23. P.M. Pinsky and N.N. Abboud, "Transient Finite Element Analysis of the Exterior Structural Acoustics Problem," *Numerical Techniques in Acoustic Radiation*, edited by R.J. Bernhard and R.F. Keltie, NCA-Vol. 6, American Society of Mechanical Engineers, New York, pp. 35-47 (1989).

24. J.T. Hunt, M.R. Knittel, and D. Barach, "Finite Element Approach to Acoustic Radiation from Elastic Structures," *J. Acoust. Soc. Amer.*, Vol. 55, pp-269-280 (1974).

25. J.T. Hunt, M.R. Knittel, C.S. Nichols, and D. Barach, "Finite-Element Approach to Acoustic Scattering from Elastic Structures," *J. Acoust. Soc. Amer.*, Vol. 57, pp. 287-299 (1975).

26. J.B. Keller and D. Givoli, "Exact Non-reflecting Boundary Conditions," *J. Comput. Phys.*, Vol. 82, pp. 172-192 (1989).

27. A. Bostrom, "Scattering of Stationary Acoustic Waves by an Elastic Obstacle Immersed in Water," *J. Acoust. Soc. Amer.*, Vol. 67, No. 2, pp. 390-398 (1980).

28. M.F. Werby and L.H. Green, "An Extended Unitary Approach for Acoustical Scattering from Elastic Structures," *J. Acoust. Soc. Amer.*, Vol. 74, pp. 625-630 (1983).

29. M.F. Werby and G.J. Tango, "Application of the Extended Boundary Condition Equations to Scattering from Fluid-Loaded Objects," *Eng. Anal.*, Vol. 5, pp. 12-20 (1988).

30. D. Ranlet, F.L. DiMaggio, H.H. Bleich, and M.L. Baron, "Elastic Response of Submerged Shells with Internally Attached Structures to Shock Loading," *Comp. Struct.*, Vol. 7, No. 3, pp. 355-364 (1977).

31. T.L. Geers, "Doubly Asympototic Approximations for Transient Motions of Submerged Structures," *J. Acoust. Soc. Amer.*, Vol. 64, No. 5, pp. 1500-1508 (1978).

32. H.C. Neilson, G.C. Everstine, and Y.F. Wang, "Transient Response of a Submerged Fluid-Coupled Double-Walled Shell Structure to a Pressure Pulse," *J. Acoust. Soc. Amer.*, Vol. 70, No. 6, pp. 1776-1782 (1981).

33. "NASTRAN User's Manual," 1986, NASA SP-222(08), Computer Software Management and Information Center (COSMIC), University of Georgia, Athens, Georgia.

34. G.C. Everstine, "Structural Analogies for Scalar Field Problems," *Int. J. Num. Meth. in Engrg.*, Vol 17, pp. 471-476 (1981).

35. G.C. Everstine, R.S. Cheng, and S.A. Hambric, "Finite Element Solution of Transient Fluid-Structure Interaction Problems," *Nineteenth NASTRAN Users' Colloquium*, NASA CP-3111, National Aeronautics and Space Administration, Washington, DC, pp. 162-173 (April 1991).

36. A. Bayliss and E. Turkel, "Radiation Boundary Conditions for Wave-Like Equations," *Comm. Pure and Appl. Math.*, Vol. XXXIII, No. 6, pp. 707-725 (1980).

37. R.H. Cole, *Underwater Explosions*, Princeton University Press, Princeton, NJ (1948).

38. Cremer, L., Heckl, M., and Ungar, E.E., 1973, *Structure-Borne Sound*, Springer-Verlag, New York.

39. Hambric, S.A., 1990, "Power Flow and Mechanical Intensity Calculations in Structural Finite Element Analysis," *Journal of Vibration and Acoustics*, Vol. 112, No. 4, pp. 542-549.

REPORT DOCUMENTATION PAGE

Form Approved
OMB No. 0704-0188

1. AGENCY USE ONLY (Leave blank)	2. REPORT DATE	3. REPORT TYPE AND DATES COVERED
	April 1992	Conference Publication

4. TITLE AND SUBTITLE
Twentieth NASTRAN® Users' Colloquium

5. FUNDING NUMBERS

6. AUTHOR(S)

7. PERFORMING ORGANIZATION NAME(S) AND ADDRESS(ES)
COSMIC, NASA's Computer Software Management and Information Center
The University of Georgia
Athens, GA 30602

8. PERFORMING ORGANIZATION REPORT NUMBER

9. SPONSORING/MONITORING AGENCY NAME(S) AND ADDRESS(ES)
National Aeronautics and Space Administration
Washington, DC 20546

10. SPONSORING/MONITORING AGENCY REPORT NUMBER
NASA CP-3145

11. SUPPLEMENTARY NOTES
Also available from COSMIC, Athens, GA 30602

12a. DISTRIBUTION/AVAILABILITY STATEMENT
Unclassified - Unlimited

Subject Category 39

12b. DISTRIBUTION CODE

13. ABSTRACT *(Maximum 200 words)*
This publication contains the proceedings of the Twentieth NASTRAN® Users' Colloquium held in Colorado Springs, CO., April 27 through May 1, 1992. It provides some comprehensive general papers on the application of finite elements in engineering, comparisons with other approaches, unique applications, pre- and postprocessing with other auxiliary programs, and new methods of analysis with NASTRAN.

14. SUBJECT TERMS
NASTRAN, structures, structural analysis, finite element analysis, colloquium

15. NUMBER OF PAGES
188

16. PRICE CODE
A09

17. SECURITY CLASSIFICATION OF REPORT	18. SECURITY CLASSIFICATION OF THIS PAGE	19. SECURITY CLASSIFICATION OF ABSTRACT	20. LIMITATION OF ABSTRACT
Unclassified	Unclassified	Unclassified	Unlimited